Geoid
Journal of Geodesy and Geomatics

Geoid Vol. 20, No. 2, 2025, 45-59

P-ISSN: 1858-2281; E-ISSN: 2442-3998

Change Detection of Topographic Features using Iteratively Reweighted Multivariate Alteration Detection and Random Forest Classification for Partial Updating of Indonesian Topographic Map

Endang Purwati, Harintaka*
Geodetic Engineering Department, Faculty of Engineering, Universitas Gadjah Mada, Yogyakarta, 55281, Indonesia
*Corresponding author: harintaka@ugm.ac.id

Received: 09 July 2025; Revised: 18 August 2025; Accepted: 02 September 2025; Published: 06 October 2025

Abstract: The current demand for geospatial information is increasingly urgent across various sectors, making the provision of base maps a top priority that is currently being accelerated. However, a major challenges faced today is the outdated nature of the Indonesian Topographic Map (Peta Rupabumi Indonesia/RBI), many of which were produced several years ago and are now considered obsolete. Updating the data is essential to ensure the validity of geospatial information in accordance with current conditions. At present, the detection of change in topographic feature is still largely conducted manually, thereby necessitating the exploration of methods to accelerate partial map updating processes. This study implements a change detection approach using Iteratively Reweighted Multivariate Alteration Detection (iMAD) method, in combination with Random Forest (RF) and Rule-based Classification. The iMAD technique is relatively insensitive to radiometric differences between acquisition times and simultaneously considers all spectral bands. Its iterative process improves accuracy, making it suitable for change detection in partial mas updates. Random Forest Classification supports the interpretation of iMAD results by providing information on changes in land cover types. The iMAD results indicate that the majority of detected changes fall under the ambiguous category (49,18%), followed by unchanged pixels (24,78%), significant changes (20,91%), and agricultural changes (5,13%). Overall accuracy of Random Forest Classification reached 90,45 % in 2019 and 93,20 % in 2023. The Kappa coefficient was 0,8920 and 0,8936 for 2019 and 2023, respectively. The final change detection results, after applying rule-based classification show that 19,70% of the study area experienced change, while 80,30% remained unchanged. Therefore, this approach presents an effective and efficient alternative for conducting partial updates of the Indonesian Topographic Map (RBI).

Keywords: Partial Updating Maps ; Random Forest Classification; Change Detection; iMAD; Sentinel-2 Imagery

How to cite: Purwati, E., Harintaka. (2025). Change Detection of Topographic Features using Iteratively Reweighted Multivariate Alteration Detection and Random Forest Classification for Partial Updating of the Indonesian Topographic Map. *Geoid*. 20(2), 45-59.

Introduction

The need for Geospatial Information is currently very urgent for various sectors, ranging from national to regional levels. One of the national priorities that must be met is the Regional Spatial Plan. In various sectors, maps play a crucial role, especially in the planning process. Law Number 11/2020, Article 20, paragraph 5 states that Basic Geospatial Information (*Informasi Geospasial Dasar*-IGD) is gradually and systematically collected for the entire territory of Indonesia and is updated periodically within a certain period of time or at any time if needed (Pemerintah Indonesia, 2020). Government Regulation Number 45 of 2021 concerning the implementation of Geospatial Information, article 114 states that the updating of IGD is carried out within a certain period of time, at the earliest every 1 (one) year and the latest every five years (Pemerintah Indonesia, 2021). This is clarified in BIG Regulation Number 18/2021 of procedures for organizing Geospatial Information.

Article 56 of BIG Regulation Number 18/2021 states that the Implementation of Geospatial Information stipulates that the mechanism of topographic map updating is carried out if there are changes in the elements of the base map in the form of changes in position, geometric shape and/or attribute information. Fulfilling the need for base maps is a top priority that is being accelerated by the Geospatial Information Agency (*Badan Informasi Geospasial*-BIG). A further challenge currently encountering is that the data in Indonesian

Topographic Maps (*Peta Rupabumi Indonesia*-RBI) is often outdated. Based on these conditions, updating the topographic map is essential to ensure the geospatial information contained within is accurate and up-to-date. As of now, the updated implementation has been carried out entirely only at specific locations. However, information within RBI typically changes partially, impacting only particular elements and areas. Presently, the practical detection of these changes in RBI elements is still performed manually. This causes the activities carried out so far to require a lot of resources and time. Therefore, a deeper updating exploration method is needed to accelerate the partial updating method. By doing so, it is expected that the needs can be met immediately and technical implementation can be carried out effectively and efficiently.

With technological advancements, numerous data is now easily accessible and usable for updating the topographical map (Cantemir et al., 2016). Landscape appearances continuously change over time, and change detection helps make the map updating process more efficient (Duncan & Smit, 2012). Furthermore, technological developments in remote sensing continue to grow, increasing data availability. This opens up significant opportunities in machine learning and data science (Yuan et al., 2020). Geospatial data itself is also experiencing technological advancements, leading to better spatial, spectral, and temporal resolution (Izquierdo-Verdiguier & Zurita-Milla, 2020). Beyond advancements in data acquisition, a key challenge moving forward lies in data processing technology, ensuring data can be effectively utilized.

Producing up-to-date data and information requires significant resources. Therefore, breakthroughs are needed to address and expedite these requirements. Nowadays, access to the open license topographic map data and numerous cloud computing platforms is also widely available. The utilization of these data and the platforms should be maximally implemented. These technological advancements are hoped could facilitate the provision of accurate and up-to-date geospatial information.

Change detection is the process of identifying changes in the condition of objects or phenomena by observing them at different times (Singh, 1989). Multitemporal image registration, radiometric correction, and atmospheric correction are crucial considerations during the pre-processing phase of change detection. There are two primary approaches to change detection (Lu et al., 2004). They are analyzing comparisons of independent classification results from data acquired on different dates and simultaneously analyzing multitemporal data. To determine where changes have occurred, it is necessary to set a threshold to differentiate between areas that have changed and those that have not (Singh, 1989).

One robust method for change detection is Multivariate Alteration Detection (MAD). MAD is unaffected by sensor calibration and radiometric influences (Nielsen et al., 1998). Nielsen, Conradsen, and Simpson initiated and developed the MAD change detection method using a statistical approach that does not rely on classification. In this method, two multitemporal datasets are combined using Canonical Correlation Analysis (CCA) to generate MAD variable pairs that contain maximum change information (Nielsen et al., 1998). Subsequently, MAD was further developed through iterations of the MAD transformation, where pixel weighting is applied. The challenge in change detection is the radiometric and sensor differences between multitemporal images, which necessitate radiometric normalization. To address this, the Iteratively reweighted Multivariate Alteration Detection (iMAD) method can identify pixels that haven't changed. These unchanged pixels are then used for linear regression to adjust radiometric values between images (Canty & Nielsen, 2008).

Methodology

Research Location and Data

The research was conducted in parts of Yogyakarta Special Region and Central Java, situated between 7°45'00" S and 8°00'00" S latitude, and 110°00'00" E and 110°15'00" E longitude (see Figure 1). This location was chosen due to its significant development, marked by the construction of various strategic projects, including the Yogyakarta International Airport (YIA). The increasing annual population growth has led to a greater need for land-use conversion (Wibowo & Harintaka, 2023). This development has driven substantial changes in land use, such as the conversion of agricultural land and green spaces into residential, industrial, and commercial areas (Utami et al., 2023).

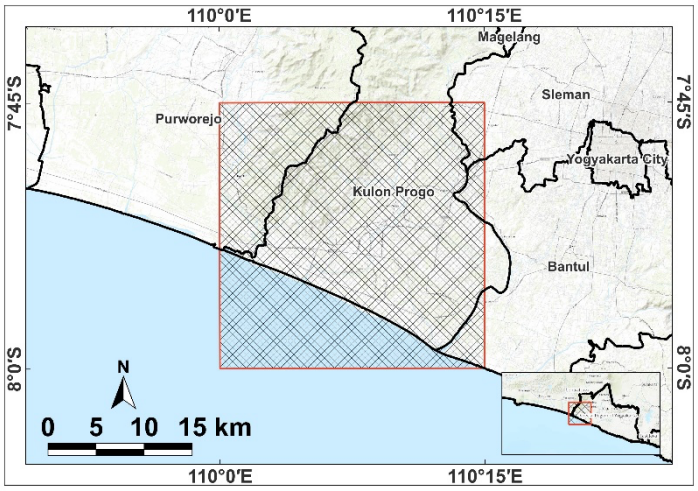

Figure 1. Research Location (Source: ESRI basemap, accessed January 2025, processed by the author)

The data used in this research is multitemporal Sentinel-2 Level 2A imagery. Sentinel-2 imagery offers excellent data volume, with a spatial resolution of up to 10 meters, good spectral resolution, and a high temporal resolution of five days (Vuolo et al., 2018). The Sentinel-2 satellite achieves its high spatial, spectral, and temporal resolution because of its specialized Multispectral Instrument (MSI) sensor (Zhang et al., 2021). Sentinel-2 imagery can achieve over 80% accuracy using supervised classification (Murayama & Ranagalage, 2020). Since this imagery has already undergone geometric and radiometric correction, only cloud masking is required for further correction (Murayama & Ranagalage, 2020).

Sentinel-2 imagery offers varying spatial resolutions, or Ground Sampling Distances (GSD). Bands 2 (blue), 3 (green), 4 (red), and 8 (NIR) provide a GSD of 10 meters. Bands 5, 6, 7, 8A, 11, and 12 have a GSD of 20 meters. Conversely, bands 1, 9, and 10 exhibit a spatial resolution of 60 meters. For this research, Sentinel-2 imagery from 2019 (T1) and 2023 (T2) was utilized. These datasets were readily available through the open-source Google Earth Engine (GEE) online catalog. The specific Sentinel-2 imagery employed in this study is illustrated in Figure 2.

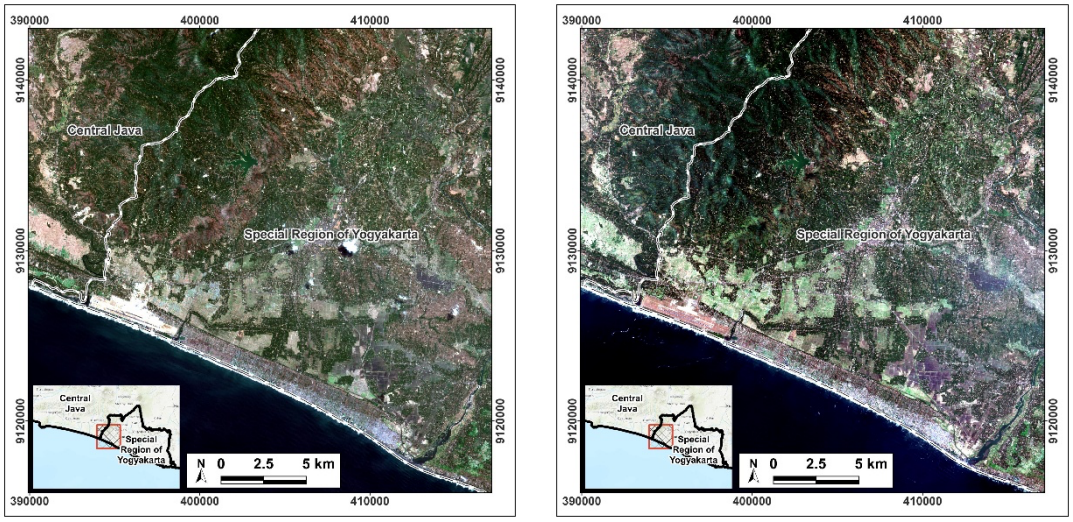

(a) (b)

Figure 2. (a) Sentinel-2 Imagery, 2019 (b) Sentinel-2 Imagery, 2023
(Source: Sentinel-2 Imagery, 2019 and 2023; processed by the author)

Research Method

The main goal of this study is to pinpoint areas within the research location that experienced land cover changes over four years, from 2019 to 2023. The results of this change detection will serve as a basis for prioritizing

updates of RBI elements. Broadly, this research involves two types of data processing: change detection and supervised classification. Figure 3 shows the overall research flowchart. For change detection, the Iteratively Reweighted Multivariate Alteration Detection (iMAD/IR-MAD) method was employed. The raw change detection results required further processing for in-depth analysis, which involved Random Forest supervised classification and subsequent rule-based classification. Both the change detection and land cover classification processes leveraged Google's cloud computing platform. This platform offers extensive storage, access, and data analysis capabilities on high-capacity servers (Amani et al., 2020).

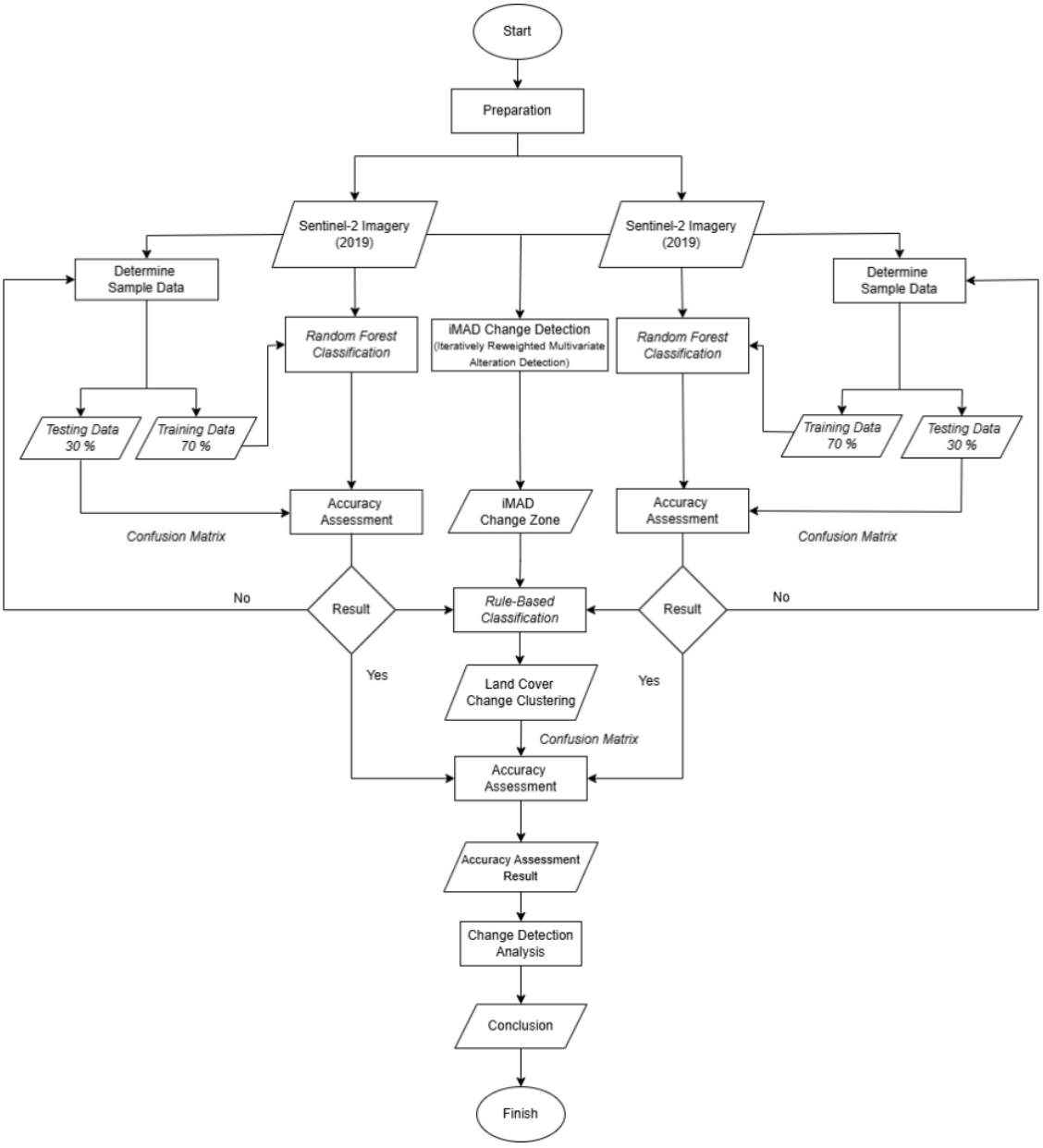

Figure 3. Research Flowchart

1. Iteratively Reweighted Multivariate Alteration Detection (iMAD/IR-MAD)

   For this research, the change detection processing is based on the Multivariate Alteration Detection (MAD) theory, as presented by (Nielsen et al., 1998). This method was later refined into Iteratively Reweighted Multivariate Alteration Detection (iMAD/IR-MAD) (Nielsen, 2007). Over time, this method has proven compatible with various software advancements, as demonstrated by (Canty & Nielsen, 2012). The stages for performing change detection using the iMAD method are as follows:

a. Simple Differencing

Change detection on two multitemporal images is performed by differencing the Sentinel-2 imagery from 2019 and 2023. To calculate the difference between the first dataset (T1) and the second dataset (T2), the following formula is used:

$$Z = X - Y \quad (1)$$

$$X = \begin{pmatrix} X_1 \\ X_2 \\ \vdots \\ X_N \end{pmatrix}, \quad Y = \begin{pmatrix} Y_1 \\ Y_2 \\ \vdots \\ Y_N \end{pmatrix} \quad (2)$$

where X is a vector representing the first dataset (T1), comprising N variables or bands. Meanwhile Y is a vector representing the second dataset (T2) with an identical structure. Z indicates the direct difference obtained by subtracting the corresponding elements of X and Y.

To derive change information and ascertain significant alterations, a decision threshold is indispensable. This threshold is typically expressed by the standard deviation of the mean difference value. The variance for each band of the image difference is calculated as follows:

$$var(Z_i) = var(X_i - Y_i) = var(X_i) + var(Y_i) - 2 \cdot cov(X_i, Y_i), \quad i = 1 \dots N, \quad (3)$$

Z_i represents the difference between the values of the i-th band at two distinct times $Z_i = X_i - Y_i$. Meanwhile $var(Z_i)$ the difference between the i-th band. The variance of the values in the i-th band at the first time point is symbolized as $var(X_i)$, and the i-th band at the second time point is $var(Y_i)$ The covariance between the i-th band from the first time point and the second time point is $cov(X_i, Y_i)$.

b. Canonical Correlation Analysis (CCA)

At this stage, a linear combination is created for all bands in both the T1 imagery (designated as U) and the T2 imagery (designated as V), forming a scalar image for each. Images U and V are made as similar as possible by selecting appropriate linear combinations before they are compared (subtracted). Similar pixels represent areas where no change has occurred, thereby allowing actual changes to appear more distinctly in the difference image. To quantify the differences in pixels that have changed, the canonical correlation coefficient between the linear combinations of T1 and T2 data must be calculated using the following formula:

$$\rho = \frac{cov(U,V)}{\sqrt{var(U)}\sqrt{var(V)}} \quad (4)$$

Where ρ represents the canonical correlation coefficient between the two linear combinations U and V. $var(U)$ dan $var(V)$ are the variances of the respective linear combinations. $U\ dan\ V$ This is standardized to 1, resulting in:

$$var(U) = var(V) = 1 \quad (5)$$

c. Generalized Eigenvalue (geneiv)

After performing Canonical Correlation Analysis (CCA), the next step is the Generalized Eigenvalue (geneiv) process. This is used to identify the linear combinations of two sets of multivariate variables that exhibit the strongest correlation, utilizing the following formula:

$$CX = \lambda BX \quad (6)$$

Where C represents the cross-covariance matrix between the two multivariate datasets (T1 dan T2), sedangkan X is the eigenvector, which constitutes the canonical weights that will form the linear combinations, λ denotes the eigenvalue, corresponding to the squared canonical correlation ($\lambda = \rho^2$). Lastly, B is the covariance matrix of one of the variable sets.

d. MAD Transformation

The MAD transformation produces several MAD layers, with each layer reflecting changes between bands that have a high correlation. The MAD transformation is calculated using the following formula:

$$M_i = U_i - V_i, \quad i = 1 \dots N, \tag{7}$$

$M_i$represents the i-th MAD component, which is the result of the difference between two linear combinations. U_i is the linear combination derived from the first time-point image (T1) and V_i is the linear combination from the second time-point image (T2).

e. Chi-square Calculation

The chi-square value represents the total degree of change at each pixel, where each MAD band has a different variance. To calculate the magnitude of change, use the following formula:

$$Z = \sum_{i=1}^{N} \left(\frac{M_i}{\sigma M_i}\right)^2 \tag{8}$$

Z represents the total χ^2 statistic or a given pixel, indicating the magnitude of the combined change. M_i is the i-th MAD component, and σM_i is the standard deviation of the i-th MAD component.

f. Iterative Reweighting

This weighting process uses the chi-square values to repeatedly calculate the canonical correlation (through n iterations) until convergence. This iteration increases sensitivity to small changes. The covariance matrix of the MAD components is defined as follows:

$$\Sigma_M = \begin{pmatrix} \sigma^2_{M_1} & 0 & \cdots & 0 \\ 0 & \sigma^2_{M_2} & \cdots & 0 \\ \vdots & \vdots & \cdots & 0 \\ 0 & 0 & \cdots & \sigma^2_{M_N} \end{pmatrix} \tag{9}$$

The chi-square statistic for change detection is calculated as follows:

$$Z = \sum_{i=1}^{N} \left(\frac{M_i}{\sigma M_i}\right)^2 \tag{10}$$

With each component's variance calculated using the following formula:

$$\sigma^2_{M_i} = var(U_i - V_i) = 2(1 - \rho_i), \quad i = 1 \dots N, \tag{11}$$

In this context, Σ_M represents the covariance matrix of the MAD components. The value Z is the χ^2 statistic obtained by summing the squares of the MAD values, each divided by its standard deviation; this value is used to detect pixels that have undergone significant change. Furthermore, $\sigma^2_{M_i}$ represents the variance of the difference between the two canonical components, U_i dan V_i which is directly related to the canonical correlation coefficient.

g. Clustering

Clustering iMAD values into several groups helps separate actual changes from noise (Nielsen, 2007). We identify the types of change within these iMAD values using K-Means unsupervised classification, which filters out ambiguous changes and helps create a binary change map (Canty & Nielsen, 2008). The iMAD results are divided into four clusters: significant change, agriculture, ambiguous change, and no change. This clustering groups similar changes together, allowing for further analysis. The significant change cluster clearly indicates notable alterations. The agriculture cluster represents changes influenced by seasonal land use patterns, requiring additional investigation. Finally, the ambiguous change cluster consists of changes with inconsistent patterns that necessitate further analysis using supplementary data.

2. Random Forest Classification

The Random Forest method is used to classify land cover and gain information about the types of land cover in the research area. During the preparation, in addition to literature review and data selection, the land cover classes are defined for the classification process. According to Indonesian National Standard (*Standar Nasional Indonesia*- SNI) No 7645:2010 on land cover classification, for maps at scales of 1:50,000 or 1:25,000, land cover is divided into five Level Two classes: agricultural areas, non-agricultural

areas, bare land, residential and related non-agricultural land, and water (Badan Standardisasi Nasional (BSN), 2010).

The land cover classes for this study are based on the Decision of the Head of the Geospatial Information Agency Number 121.4/2024. This document outlines the classification of land cover elements for Indonesian Topographic Maps across various scales, 1:1.000, 1:5.000, 1:25.000, 1:50.000, 1:250.000, 1:500.000, and 1:1.000.000. Specifically, the classes at the 1:500,000 scale were referenced. These include: built-up land, cultivated bare land, wet agricultural land, dry agricultural land/plantations, forest and natural vegetation, natural/semi-natural bare land, and water bodies (Badan Informasi Geospasial (BIG), 2024). After adjusting for the specific data conditions and visual interpretability, this research ultimately utilized eight distinct land cover classes: built-up area, road, wet paddy field, green paddy field, cropland, forest, bare land, and water body.

Random Forest is a collection of decision trees trained using specific datasets. The final result is determined by a voting process among these individual trees (Harto & Basuki, 2021). Training data was prepared for each dataset, ensuring a proportional distribution across all land cover classes. Random Forest classification was performed on the Google Earth Engine Platform, a data split of 70% for training and 30% for testing achieved an accuracy of 94% (Matarira et al., 2022). For this research, a total of 436 samples were used for the 2019 data and 443 samples for the 2023 data as training data. The composition of the training data for each land cover class is presented in Table 1.

Table 1. Random Forest Supervised Classification Training Data

Land Cover Classes	Training Sample Size (2019)	Training Sample Size (2023)
Built-up Area	51	52
Road	36	52
Green Paddy Field	48	58
Wet Paddy Field	50	57
Cropland	68	65
Forest	56	67
Bare Land	63	60
Water Body	64	62

3. Rule-Based Classification

The iMAD change detection results were analyzed in conjunction with the Random Forest classification outcomes to ascertain the nature of land cover alterations. When integrating iMAD and Random Forest results, inconsistencies were frequently observed. For instance, an iMAD result might indicate a change in a group of pixels; however, a comparison with the Random Forest classifications for T1 and T2 could reveal no actual change for those same pixels. Conversely, another scenario involved pixels identified as changed by both iMAD and the Random Forest classifications for T1 and T2, yet this alteration might be attributable to seasonal variations rather than a permanent shift. Such cases are particularly prevalent in agricultural regions. For pixels within the ambiguous change cluster, the land cover type information derived from the T1 and T2 classification results served as the definitive basis for determining whether a pixel had alteration.

Based on these conditions, post-detection classification is necessary, applying several conditional requirements and utilizing additional data. This classification is crucial for filtering ambiguous change areas (Lu & Weng, 2007). The criteria for identifying change are presented in Table 2.

Table 2. Change Criteria

Land Cover Types		2023								Cluster
		Built-up Area	Road	Green Paddy Field	Wet Paddy Field	Cropland	Forest	Bare Land	Water Body	
2019	Built-up Area	UC	C	C	C	C	C	C	C	Cluster 0 (Significant Change)
	Road	C	UC	C	C	C	C	C	C	
	Green Paddy Field	C	C	UC	C	C	C	C	C	
	Wet Paddy Field	C	C	C	UC	C	C	C	C	
	Cropland	C	C	C	C	UC	C	C	C	
	Forest	C	C	C	C	C	TC	C	C	
	Bare Land	C	C	C	C	C	C	UC	C	
	Water Body	C	C	C	C	C	C	C	UC	
	Built-up Area	UC	C	C	C	C	C	C	C	Cluster 1 (Agricultural Change)
	Road	C	UC	C	C	C	C	C	C	
	Green Paddy Field	C	C	UC	UC	UC	UC	UC	C	
	Wet Paddy Field	C	C	UC	UC	UC	C	UC	UC	
	Cropland	C	C	UC	UC	UC	C	UC	C	
	Forest	C	C	UC	C	C	UC	C	C	
	Bare Land	C	C	UC	UC	UC	C	UC	C	
	Water Body	C	C	C	UC	C	C	C	UC	
	Built-up Area	UC	C	C	C	C	C	C	C	Cluster 2 (Ambiguous Change)
	Road	C	UC	C	C	C	C	C	C	
	Green Paddy Field	C	C	UC	C	C	C	C	C	
	Wet Paddy Field	C	C	C	UC	C	C	C	C	
	Cropland	C	C	C	C	UC	C	C	C	
	Forest	C	C	C	C	C	UC	C	C	
	Bare Land	C	C	C	C	C	C	UC	C	
	Water Body	C	C	C	C	C	C	C	UC	
	Built-up Area	UC	UC	UC	UC	UC	UC	UC	UC	Cluster 3 (Unchanged)
	Road	UC	UC	UC	UC	UC	UC	UC	UC	
	Green Paddy Field	UC	UC	UC	UC	UC	UC	UC	UC	
	Wet Paddy Field	UC	UC	UC	UC	UC	UC	UC	UC	
	Cropland	UC	UC	UC	UC	UC	UC	UC	UC	
	Forest	UC	UC	UC	UC	UC	UC	UC	UC	
	Bare Land	UC	UC	UC	UC	UC	UC	UC	UC	
	Water Body	UC	UC	UC	UC	UC	UC	UC	UC	

Table 2 outlines the criteria for the results from iMAD, which will undergo further classification using a rule-based classification method. The table's cluster column contains four conditions or clusters that were previously explained. The rows and columns representing land cover types are the result of a random forest classification from 2019 (T1) and 2023 (T2). These are divided into eight land cover types: Built-up areas, Roads, Green rice fields, Wet rice fields, Croplands, Forests, Bare lands, and Water bodies. The criteria for determining change involve three conditions: the iMAD cluster results, the land cover type in T1 (2019), and the land cover type in T2 (2023). Applying these criteria will produce two final classes: Changed (C) and Unchanged (UC).

4. Accuracy Assessment of Change Detection Results

For accuracy assessment, a minimum sample size of 50 to 75 pixels per class is recommended. If sufficient data is available, it is preferable to use 100 to 200 pixels per class (Congalton & Green, 2019). The number of samples for accuracy assessment can also be determined based on the area size per class, with an ideal number of 500 to 1000 test points for areas exceeding 10,000 km² (Olofsson et al., 2014). In this research, the accuracy of the rule-based classification results will be assessed using a confusion matrix. This matrix will be generated from visual interpretation of T1 and T2 data sources, utilizing a total of 250 sample points, with distribution per cluster as shown in Table 3.

Table 3. Accuracy Assessment Points for Change Detection Results

Cluster	Numbers of Assessment Points
Significant Change	59
Agricultural Change	62
Ambiguous Change	69
Unchanged	60
Total	**250**

Results and Discussion

This section presents the outcomes of utilizing the iMAD change detection method, RF classification algorithm, and rule-based classification. The iMAD methodology produces a change component that highlights multivariate statistics between T1 and T2 (Nielsen, 2007; Pathak, 2014), whereas RF is employed to classify land cover types based on spectral characteristics (Nguyen et al., 2018; Rodriguez-Galiano et al., 2012). To enhance the outcomes of the change component, post-classification is conducted (Liu & Zhou, 2004; Zhou et al., 2008). In this study, post-classification is implemented using rule-based classification using spatial logic and interclass interactions.

Iteratively Reweighted Multivariate Alteration Detection (iMAD/IR-MAD)

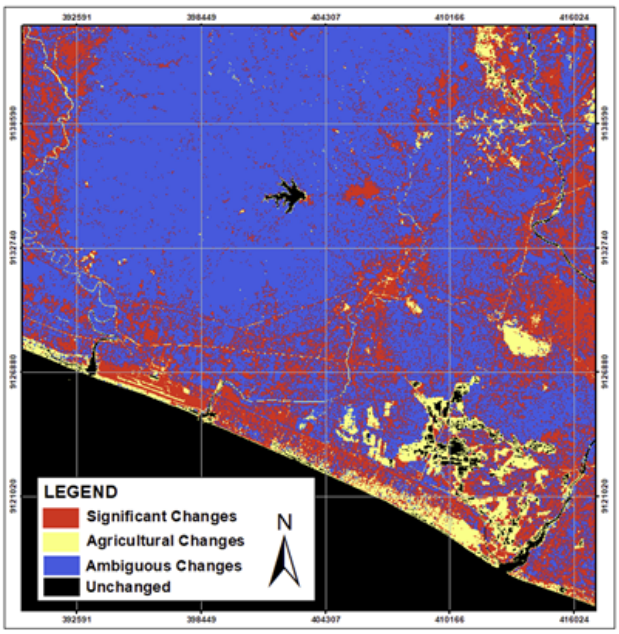

Figure 4. iMAD *(*Iteratively Reweighted Multivariate Alteration Detection*)* Results
(Source: Sentinel-2 Image of 2019 and 2023, processed by the Author)

Figure 4 illustrates the outcome of change detection employing the iMAD (Iteratively Reweighted Multivariate Alteration Detection) technique. This method yields pixels that vary and remain constant. The clustering technique categorizes these conditions into four distinct clusters. The cluster with substantial alterations is denoted by a red. The cluster of agricultural transformation is shown in yellow. The blue colour signifies the aggregation of ambiguous alterations. Meanwhile, unchanged pixels are denoted by black. The iMAD results indicated that 49.18% of total pixels are classified as ambiguous changes, 24.78% as unchanged pixels, 20.91% of total pixels as significant changes, and 5.13% of total pixels as agricultural changes.

Numerous coastal regions have been identified as undergoing agricultural changes. The area surrounding YIA airport has been identified as experiencing substantial changes and agriculture changes. Meanwhile, most of the sites identified as stable are water areas, specifically the ocean and reservoirs. Ambiguous changes are the largest change detection result. This underscores the necessity for additional classification through rules-based methods to ensure clear identification.

The iMAD technique incorporates multi-bands sensitive to variations in plant and soil, specifically bands B5, B6, B7, B8A, B11, and B12, with a spatial resolution of 20 meters (Canty, 2014; Canty & Nielsen, 2008). The iMAD results on the Sentinel-2 images has a spatial resolution of 20 meters. The RF classification was generated at a spatial resolution of 10 meters, as it is trained on a band with a resolution of 10 meters. The disparity in spatial resolution between iMAD and RF data posed a spatial challenge during collaboration. This may lead to discrepancies between the changes detection result and RF classification outcomes, hence impacting the spatial accuracy of the combined classification results (Nielsen, 2007). Figure 5 illustrated the disparity in spatial resolution between iMAD and RF results, where in a single cluster of iMAD results encompasses several categories of RF land cover.

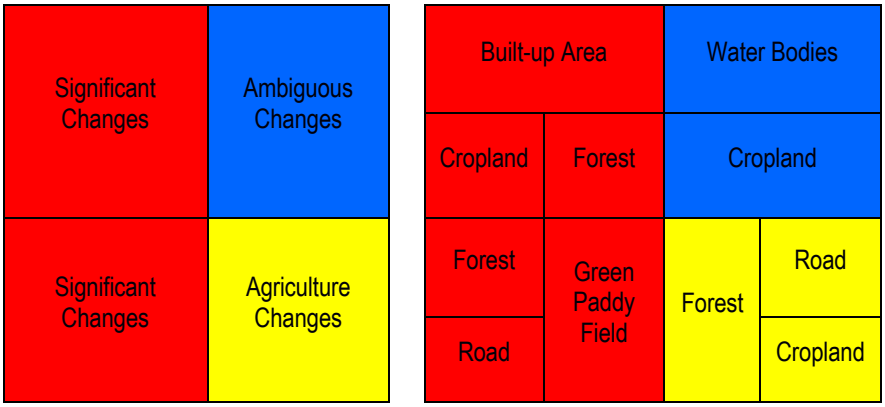

(a) (b)

Figure 5. Pixel Illustration (a) *iMAD* Results, (b) *Random Forest Classification Results*
(Source: Data Processing, 2025)

Random Forest Classification

The classification of random forests carried out on multitemporal images in 2019 (T1) and 2023 (T2) produced two outputs with different accuracy values. Figure 6 (a) shows the results of the 2019 random forest classification, while Figure 6 (b) shows the results of the 2023 random forest classification.

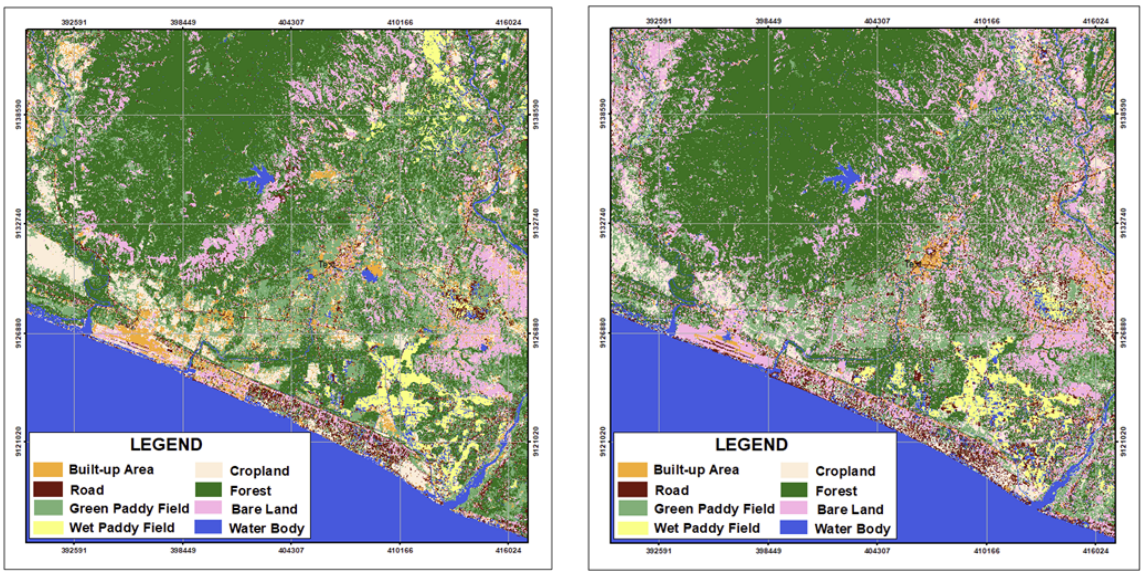

(a) (b)

Figure 6. Random Forest Classification Results (a) 2019, (b) 2023
(Source: Sentinel-2 Images of 2019 and 2023, processed by the Author)

Table 4 presents the accuracy values of the RF Classification on T1 and T2. The classification results has an overall accuracy of 90.45% in 2019 and 93.20% in 2023. The Kappa coefficient was is 0.8902 for the RF classification in 2019 and 0.8936 for the 2023 classification results. Other accuracy indicators for T1 and T2 results are included in Table 4.

Table 4. Accuracy of *Random Forest Classification Result*

Accuracy Indicator	T1 (2019)	T2 (2023)
Overall Accuracy	90.45%	93.20%
Producer Accuracy	91.44%	86.67%
User Accuracy	90.67%	84.12%
Kappa Coefficient	0.8902	0.8936
F-Score	0.9106	0.8537

Image classification accuracy is considered very good if it has accuracy value of ≥ 90%, accuracy value between 80-89% is categorized as good, quite good with accuracy value of 70-79%, less good if it is in the range of 60-69%, and is labeled as bad if the accuracy value is < 60% (Congalton & Green, 2009). Despite the classification results in this study is in the very good category, specifically 90.45% for RF T1 and 93.20% for RF T2, there are remain some aspects that can be analyzed. A shortcoming of Sentinel-2 image is its spatial resolution of 10 meters in the visible band. This results in the inability to classify anything smaller than 10 meters, including narrow roads, small buildings, ponds or small fishponds, and similar objects, due to mixed pixels. A situation in which a single pixel denotes more than one type of land cover (Fisher, 1997).

Figure 7 (a) illustrates the occurrence of mixed pixels on objects less than 10 meters. Distinctly observable objects include roads that are more than 10 meters in width, which classification results is symbolized by red; whilesmall roads with a size less than 10 meters are not classified in the RF results. Figure 7 (b) illustrates a region with a diverse land cover types, including built-up areas, roads, green paddy fields, forests, and bare lands. The classification results indicate that the boundary of land cover types cannot be identified clearly, resulting in a mixed and inconsistent land cover pattern. In addition to the impact of spatial resolution on the Sentinel-2 image, the selection of training areas are also significantly influenced the RF results. Training areas must be selected to ensure homogeneity so that pixels with different objects do not mix.

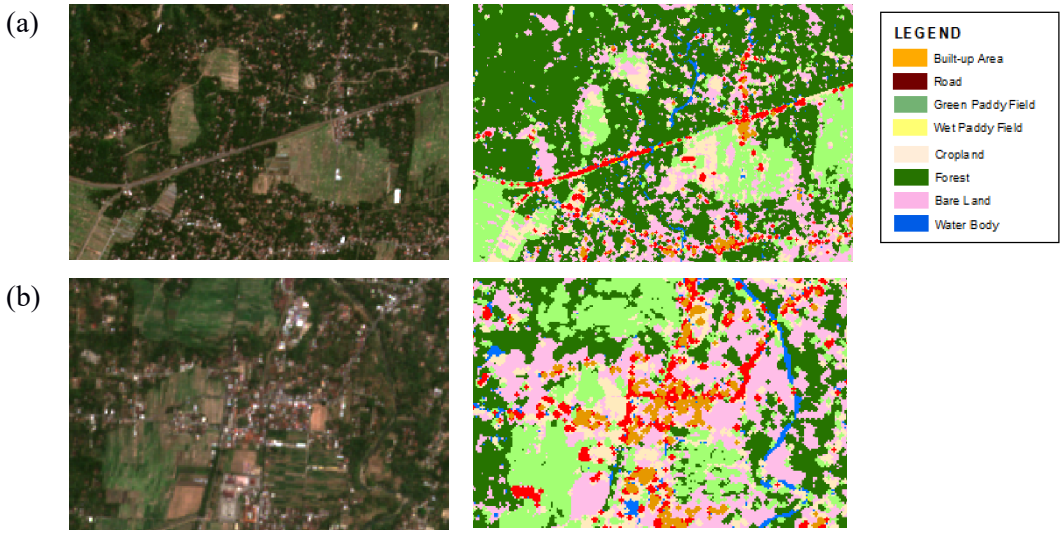

Figure 7. Mixed Pixel Conditions in RF Classification Results
(Source: Sentinel-2 images of 2023, processed by the Author)

Rule-Based Classification

Post-changed detection classification produces information regarding locations that have changed and those that remain unchanged. As illustrated in Figure 8, after applied the change detection using rule-based classsification, categorization yield substantial information in contrast to iMAD results, which are not assessed using change determination criteria. Red colour denotes a location that has changed, whereas black colour represents a location that remains unchanged. The final change detection results shows that 19.70% coverage of the research area is changed, whilst 80.30% remains unchanged.

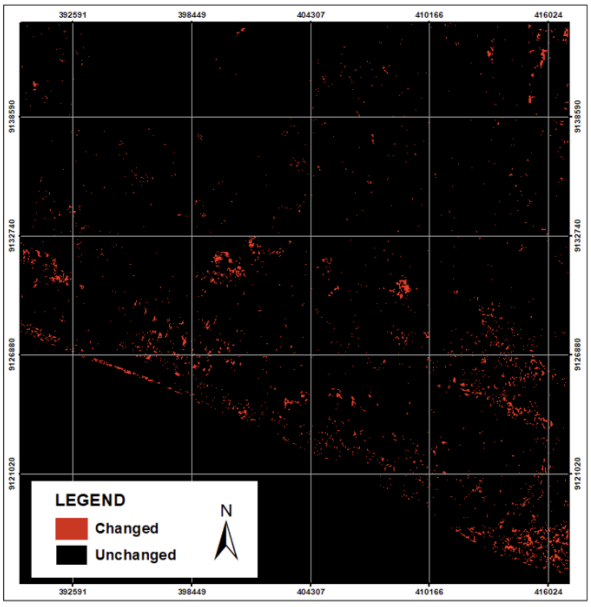

Figure 8. Change Detection Final Result
(Source: Sentinel-2 Image of 2019 and 2023, processed by the Author)

Test the Accuracy of Change Detection Results

The accuracy assessment of the post-changed detection classification results, utilizing rule-based classification, shows that the total accuracy for the 250 test points is 80.80%. Table 5 presents the accuracy of each cluster. The Significant Change cluster has the lowest accuracy value at 49.15%, with 29 out of 59 total

test points in the cluster. The Ambiguous Change cluster has the highest accuracy value at 98.55%. Only one inappropriate point was identified among 69 test points in the Ambiguous cluster. In the Agricultural Changes cluster, 51 out of 62 test points are deemed appropriate, resulting in an accuracy value of 82.26%. The iMAD results in the cluster Unchanged with an accuracy value of 90.00%. There are 6 of the tes points are inappropriate out of a total of 60 test points in this cluster.

Table 5. Test Value for Change Detection Results

Cluster	Change Detection Accuracy Test Results		Cluster Accuracy
	Appropriate	Inappropriate	
Significant Changes	29	30	49.15%
Agricultural Changes	51	11	82.26%
Ambiguous Changes	68	1	98.55%
Unchanged	54	6	90.00%

The change detection results has an accuracy value of 80.80%, categorizing as good. In the post-classification phase, utilizing rule-based classification, it can enforce the status of changes that initially comprised three clusters in the iMAD results into changed or unchanged information. If the iMAD data are utilized directly, the Significant Changes cluster, the Agricultural Changes cluster, and the Ambiguous Changes cluster will be classified into the changed category. The results cannot be immediately concluded and executed. When compared with the RF classification results for T1 and T2, they are not yet consistent, so further intervention and accuracy testing are needed.

Figure 9 shows that iMAD can identify significant changes in objects surrounding YIA Airport, including the newly observed airport railway in the 2023 Sentinel image.

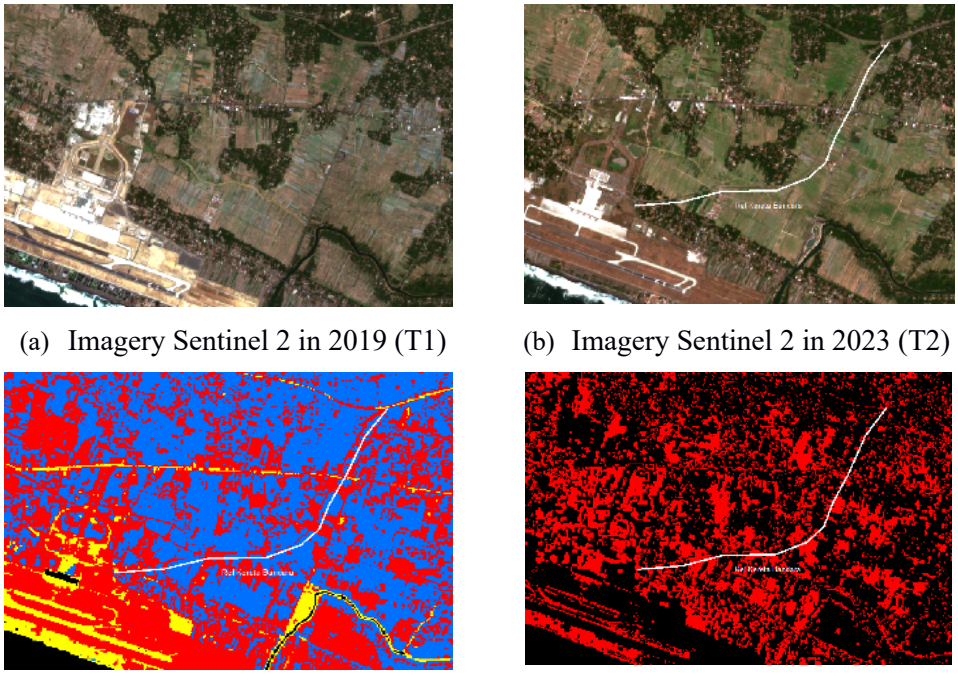

(a) Imagery Sentinel 2 in 2019 (T1) (b) Imagery Sentinel 2 in 2023 (T2)

(c) iMAD result (d) Final Change Detection Result

Figure 9. YIA Airport Train Line Object Change Detection
(Source: Sentinel Image 2 of 2019 and 2023, processed by the Author)

To address the spatial resolution discrepancies between iMAD and RF results, additional processing for resolution adjustment is required. Downsampling 10-meter image or upsampling iMAD results is an alternative to ensure consistency in spatial analysis and enhance the accuracy of change detection. Incorporating more

relevant band information in RF optimization can enhance accuracy value by 9.1%, while a 10.4% improvement is achieved using Bayesian methods (Zhang et al., 2021). The combination of iMAD with OBIA (Object-Based Image Analysis) for change detection in for the base map updates can be done for future research. (Chen et al., 2024) have integrated object analysis with multitemporal semantic change detection, specifically employing iMAD alongside its statistical variations. Simultaneously, (Ma et al., 2024) have examined diverse collaborative techniques for several development methodologies, including the integration of deep learning with Object-Based Image Analysis (OBIA) for change detection through deep change features. Lack of researches that integrates iMAD and OBIA, potentially opens up collaborative opportunities for analyzing more pixel and objects changes in the future.

Conclusion

The change detection results shows an accuracy value of 80.80%, categorized as good. The accuracy is derived from a combination of RF classification utilizing Sentinel data from 2019 and 2023, which resulted very good accuracy levels of 90.45% and 93.20%, respectively. The change detection analysis show that 19.70% of the research area has changed, whereas 80.30% of the area is remained unchanged. The iMAD approach effectively detects spectral changes in multitemporal satellite imagery using an iterative procedure that enhances sensitivity to minor changes. The combination of iMAD and RF produces spatial information on changes in RBI elements. Consequently, this method may serve as an effective and efficient alternative for the partial update of the RBI Map.

References

Amani, M., Ghorbanian, A., Ahmadi, S. A., Kakooei, M., Moghimi, A., Mirmazloumi, S. M., Moghaddam, S. H. A., Mahdavi, S., Ghahremanloo, M., Parsian, S., Wu, Q., & Brisco, B. (2020). Google Earth Engine Cloud Computing Platform for Remote Sensing Big Data Applications: A Comprehensive Review. *IEEE Journal of Selected Topics in Applied Earth Observations and Remote Sensing*, *13*, 5326–5350. https://doi.org/10.1109/JSTARS.2020.3021052

Badan Informasi Geospasial (BIG). (2024). *Keputusan Kepala Badan Informasi Geospasial Nomor 121.4 Tahun 2024 Tentang Klasifikasi Unsur Penutup Lahan untuk Peta Rupabumi Indonesia Skala 1:1.000, 1:5.000, 1:25.000, 1:50.000, 1:250.000, 1:500.000, dan 1:1.000.000*. Badan Informasi Geospasial.

Badan Standardisasi Nasional (BSN). (2010). *SNI 7645:2010 Peta Penutup Lahan*.

Cantemir, A., Visan, A., Parvulescu, N., & Dogaru, M. (2016). The use of multiple data sources in the process of topographic maps updating. *International Archives of the Photogrammetry, Remote Sensing and Spatial Information Sciences - ISPRS Archives*, *41*(July), 19–24. https://doi.org/10.5194/isprsarchives-XLI-B4-19-2016

Canty, M. J. (2014). Image Analysis, Classification and Change Detection in Remote Sensing. In *Image Analysis, Classification and Change Detection in Remote Sensing* (Fourth Edi). Taylor & Francis. https://doi.org/10.1201/b17074

Canty, M. J., & Nielsen, A. A. (2008). Automatic radiometric normalization of multitemporal satellite imagery with the iteratively re-weighted MAD transformation. *Remote Sensing of Environment*, *112*(3), 1025–1036. https://doi.org/10.1016/j.rse.2007.07.013

Canty, M. J., & Nielsen, A. A. (2012). Linear and kernel methods for multivariate change detection. *Computers and Geosciences*, *38*(1), 107–114. https://doi.org/10.1016/j.cageo.2011.05.012

Chen, H., Lan, C., Song, J., Broni-Bediako, C., Xia, J., & Yokoya, N. (2024). ObjFormer: Learning Land-Cover Changes from Paired OSM Data and Optical High-Resolution Imagery via Object-Guided Transformer. *IEEE Transactions on Geoscience and Remote Sensing*, *62*, 1–21. https://doi.org/10.1109/TGRS.2024.3410389

Congalton, R. G., & Green, K. (2009). *Assessing the Accuracy of Remotely Sensed Data: Principles and Practices* (2nd ed.). CRC Press.

Congalton, R. G., & Green, K. (2019). *Assessing the Accuracy of Remotely Sensed Data*. Taylor & Francis.

Duncan, P., & Smit, J. (2012). an Investigation of Automatic Change Detection for Topographic Map Updating. *The International Archives of the Photogrammetry, Remote Sensing and Spatial Information Sciences*, *XXXIX-B7*(September), 311–316. https://doi.org/10.5194/isprsarchives-xxxix-b7-311-2012

Fisher, P. (1997). The pixel: A snare and a delusion. *International Journal of Remote Sensing*, *18*(3), 679–685. https://doi.org/10.1080/014311697219015

Harto, M. K., & Basuki, A. (2021). Deteksi Serangan DDoS Pada Jaringan Berbasis SDN Dengan Klasifikasi Random Forest. *Jurnal Pengembangan Teknologi Informasi Dan Ilmu Komputer*, *5*(4), 1329–1333. http://j-ptiik.ub.ac.id

Izquierdo-Verdiguier, E., & Zurita-Milla, R. (2020). An evaluation of Guided Regularized Random Forest for classification and regression tasks in remote sensing. *International Journal of Applied Earth Observation and*

Geoinformation, *88*(October 2019). https://doi.org/10.1016/j.jag.2020.102051
Liu, H., & Zhou, Q. (2004). Accuracy analysis of remote sensing change detection by rule-based rationality evaluation with post-classification comparison. *International Journal of Remote Sensing*, *25*(5), 1037–1050. https://doi.org/10.1080/0143116031000150004
Lu, D., Mausel, P., Brondízio, E., & Moran, E. (2004). Change detection techniques. *International Journal of Remote Sensing*, *25*(12), 2365–2401. https://doi.org/10.1080/0143116031000139863
Lu, D., & Weng, Q. (2007). A survey of image classification methods and techniques for improving classification performance. *International Journal of Remote Sensing*, *1161*. https://doi.org/10.1080/01431160600746456
Ma, L., Yan, Z., Li, M., Liu, T., Tan, L., Wang, X., He, W., Wang, R., He, G., Lu, H., & Blaschke, T. (2024). Deep Learning Meets OBIA : Tasks , Challenges , Strategies , and Perspectives. *IEEE Geoscience and Remote Sensing Magazine*, 1–25.
Matarira, D., Mutanga, O., & Naidu, M. (2022). Google Earth Engine for Informal Settlement Mapping: A Random Forest Classification Using Spectral and Textural Information. *Remote Sensing*, *14*(20). https://doi.org/10.3390/rs14205130
Murayama, Y., & Ranagalage, M. (2020). Sentinel-2 Data for Land Cover/Use Mapping: A Review. *Remote Sensing*, *12*.
Nguyen, H. T. T., Doan, T. M., & Radeloff, V. (2018). Applying Random Forest classification to map Land use/Land cover using Landsat 8 OLI. *International Archives of the Photogrammetry, Remote Sensing and Spatial Information Sciences - ISPRS Archives*, *42*(3W4), 363–367. https://doi.org/10.5194/isprs-archives-XLII-3-W4-363-2018
Nielsen, A. A. (2007). The regularized iteratively reweighted MAD method for change detection in multi- and hyperspectral data. *IEEE Transactions on Image Processing*, *16*(2), 463–478. https://doi.org/10.1109/TIP.2006.888195
Nielsen, A. A., Conradsen, K., & Simpson, J. J. (1998). *Multivariate Alteration Detection (MAD) and MAF Postprocessing in Multispectral, Bitemporal Image Data: New Approaches to Change Detection Studies*. Elsevier Science Inc.
Olofsson, P., Foody, G. M., Herold, M., Stehman, S. V., Woodcock, C. E., & Wulder, M. A. (2014). Good practices for estimating area and assessing accuracy of land change. *Remote Sensing of Environment*, *148*, 42–57. https://doi.org/10.1016/j.rse.2014.02.015
Pathak, S. (2014). New Change Detection Techniques to monitor land cover dynamics in mine environment. *International Archives of the Photogrammetry, Remote Sensing and Spatial Information Sciences - ISPRS Archives*, *40*(8), 875–879. https://doi.org/10.5194/isprsarchives-XL-8-875-2014
Pemerintah Indonesia. (2020). *Undang-undang (UU) Nomor 11 Tahun 2020 tentang Cipta Kerja*. Pemerintah Indonesia. https://peraturan.bpk.go.id/Details/149750/uu-no-11-tahun-2020
Pemerintah Indonesia. (2021). *Peraturan Pemerintah (PP) Nomor 45 Tahun 2021 tentang Penyelenggaraan Informasi Geospasial*. Pemerintah Indonesia. https://peraturan.bpk.go.id/Details/161966/pp-no-45-tahun-2021
Rodriguez-Galiano, V. F., Ghimire, B., Rogan, J., Chica-Olmo, M., & Rigol-Sanchez, J. P. (2012). An assessment of the effectiveness of a random forest classifier for land-cover classification. *ISPRS Journal of Photogrammetry and Remote Sensing*, *67*(1), 93–104. https://doi.org/10.1016/j.isprsjprs.2011.11.002
Singh, A. (1989). Review Articlel: Digital change detection techniques using remotely-sensed data. *International Journal of Remote Sensing*, *10*(6), 989–1003. https://doi.org/10.1080/01431168908903939
Utami, W., Kuna, A., & Marini, M. (2023). Dampak Pembangunan Bandara Internasional Yogyakarta Terhadap Perubahan Penggunaan Lahan. *Jurnal Pembangunan Wilayah Dan Kota*, *19*(1), 105–117. https://doi.org/10.14710/pwk.v19i1.37429
Vuolo, F., Neuwirth, M., Immitzer, M., Atzberger, C., & Ng, W. T. (2018). How much does multi-temporal Sentinel-2 data improve crop type classification? *International Journal of Applied Earth Observation and Geoinformation*, *72*(June), 122–130. https://doi.org/10.1016/j.jag.2018.06.007
Wibowo, R. A., & Harintaka. (2023). Pembuatan Model Prediksi Lahan Terbangun di Kabupaten Kulon Progo dengan Citra Satelit Penginderaan Jauh. *Geoid*, *19*(1), 18–27.
Yuan, Q., Shen, H., Li, T., Li, Z., Li, S., Jiang, Y., Xu, H., Tan, W., Yang, Q., Wang, J., Gao, J., & Zhang, L. (2020). Deep learning in environmental remote sensing: Achievements and challenges. *Remote Sensing of Environment*, *241*(February), 111716. https://doi.org/10.1016/j.rse.2020.111716
Zhang, T., Su, J., Xu, Z., Luo, Y., & Li, J. (2021). Sentinel-2 satellite imagery for urban land cover classification by optimized random forest classifier. *Applied Sciences (Switzerland)*, *11*(2), 1–17. https://doi.org/10.3390/app11020543
Zhou, W., Troy, A., & Grove, M. (2008). Object-based land cover classification and change analysis in the baltimore metropolitan area using multitemporal high resolution remote sensing data. *Sensors*, *8*(3), 1613–1636. https://doi.org/10.3390/s8031613